Translational Stroke Research
https://doi.org/10.1007/s12975-024-01285-2

RESEARCH

An Alternative Photothrombotic Model of Transient Ischemic Attack

Kalyuzhnaya Y. N.[1] · Logvinov A. K.[1] · Pashkevich S. G.[2] · Golubova N. V.[3] · Seryogina E. S.[3] · Potapova E. V.[3] · Dremin V. V.[3] · Dunaev A. V.[3] · Demyanenko S. V.[1]

Received: 5 June 2024 / Revised: 17 July 2024 / Accepted: 22 July 2024

Abstract

Animal models mimicking human transient ischemic attack (TIA) and cerebral microinfarcts are essential tools for studying their pathogenetic mechanisms and finding methods of their treatment. Despite its advantages, the model of single arteriole photothrombosis requires complex experimental equipment and highly invasive surgery, which may affect the results of further studies. Hence, to achieve high translational potential, we focused on developing a TIA model based on photothrombosis of arterioles to combine good reproducibility and low invasiveness. For the first time, noninvasive laser speckle contrast imaging (LSCI) was used to monitor blood flow in cerebral arterioles and reperfusion was achieved. We demonstrate that irradiation of mouse cerebral cortical arterioles using a 532-nm laser with a 1-mm-wide beam at 2.4 or 3.7 mW for 55 or 40 s, respectively, after 15 mg/kg intravenous Rose Bengal administration, induces similar ischemia–reperfusion lesions resulting in microinfarct formation. The model can be used to study the pathogenesis of spontaneously developing cerebral microinfarcts in neurodegeneration. Reducing the exposure times by 10 s while maintaining the same other parameters caused photothrombosis of the arteriole with reperfusion in less than 1 h. This mode of photodynamic exposure caused cellular and subcellular level ischemic changes in neurons and promoted the activation of astrocytes and microglia in the first day after irradiation, but not later, without the formation of microinfarcts. This mode of photodynamic exposure most accurately reproduced human TIA, characterized by the absence of microinfarcts.

Keywords Transient ischemic attack · Photothrombotic model · Blood flow in cerebral arterioles · Laser speckle contrast imaging

Introduction

Circulatory disturbances in brain arteries result in the development of acute stroke and cerebral infarction; in turn, transient flow disturbances in individual arterioles, or transient ischemic attack (TIA), may or may not be associated with the formation of microinfarcts. According to the classical definition of TIA, a transient cerebral circulatory impairment is not accompanied by microinfarct formation [1]. However, microinfarcts are found in 25–40% of TIA patients via diffusion-weighted MRI [2]. Therefore, a new definition of TIA has been proposed: TIA is a brief episode of neurological dysfunction caused by a focal brain lesion with clinical symptoms, lasting typically less than 24 h, without evidence of acute infarction [3]. However, TIAs should not be considered benign. Death rate after TIA is 15% in the first year and up to 50% in the following 5 years [3, 4]. TIA significantly slows the functional recovery in post-stroke patients [5, 6]. Therefore, prevention and treatment of TIA are of high importance.

A limiting factor in the success of TIA research is that there are relatively few simple animal models with minor and recurrent lesions. The mild transient focal ischemia that occurs in TIA can be induced experimentally by brief middle cerebral artery occlusion (MCAO), causing selective cell necrosis [7, 8]. MCAO-based TIA models are challenging as they involve multiple technically demanding invasive

✉ Demyanenko S. V.
svdemyanenko@sfedu.ru

[1] Laboratory of Molecular Neuroscience, Academy of Biology and Biotechnology, Southern Federal University, 194/1 Stachki Ave, Rostov-On-Don 344090, Russia

[2] State Scientific Institution "Institute of Physiology, of the National Academy of Sciences of Belarus", Akademicheskaya Str., 28, 220072 Minsk, Belarus

[3] Research and Development Center of Biomedical Photonics, Orel State University, 95 Komsomolskaya St, Orel 302026, Russia

surgeries. An alternative is TIA models based on photothrombosis of small vessels in rodent brains. The distinct feature of all photothrombosis-based stroke models is the relatively low invasiveness and high reproducibility of the lesion [9]. After the administration of a photosensitizer, such as Rose Bengal, irradiation of blood vessels at a certain wavelength results in the generation of reactive oxygen species, mainly singlet oxygen, and, as a consequence, in endothelial cell damage and platelet activation, eventually triggering the blood clotting cascade [10].

The use of photodynamic effect allows selective occlusion of a single penetrating arteriole via clot induction using precise laser irradiation after photosensitizer administration, combined with two-photon laser scanning microscopy or laser Doppler flowmetry [11]. However, two-photon excitation-based TIA models require complex experimental equipment, and the surgical procedure itself is highly invasive due to the requirement of cranial window formation, which significantly increases the probability of inflammatory reactions and animal mortality, preventing modeling of recurrent TIAs. The loss of blood flow even in a single cortical penetrating arteriole often causes a cylindrical microinfarction that can extend to the entire depth of the cortical substance [12].

An alternative is models where irradiation is applied through a thinned skull. For example, a minor stroke can be reproduced using a low-intensity laser beam with a bright center at a low dose of Rose Bengal photosensitizer and a short, 5 to 15-min illumination of the rat's thinned skull [13, 14]. Using this approach allows for the study of recurrent minor stroke due to relatively technically simple manipulations [13]. However, when using unfocused lasers, the infarct volume may be more significant compared to that in human TIAs due to thrombosis of multiple microvessels and the inability to achieve controlled reperfusion, as well as due to microvascular rupture.

When testing expensive new drugs in vivo, it is important to use the lowest possible dose, so it is preferable to perform drug studies or inhibitor assays in mice. In addition, genetically modified lines of mice, rather than rats, are often used for research. Mice are less expensive to keep than rats, so they are preferred for adult animal studies. However, collateral blood flow in the mouse brain varies between mouse lines, leading to variability in clinical outcomes and stroke size [15] and creating difficulties in modeling TIA and minor stroke in mice.

All currently available mouse models of TIA are based on temporary blockage of blood flow via irradiation of single penetrating arteries with high-energy impulse lasers after forming a cranial window with the formation of superficial or deep microinfarcts, which often leads to dissection of the target vessel with subsequent microbleeding [9]. Therefore, to achieve high translational potential, it is necessary to develop an optimal TIA model that combines the advantages and addresses the disadvantages of the available models, combining good reproducibility and low invasiveness.

Taking into account the experience of our colleagues and the available limitations, we propose a new variant of a mouse model of TIA with microinfarct formation and spontaneous restoration of blood flow in the cerebral arteriole without microinfarct formation. The strategy we suggest utilizes a widely available diode green laser and does not require the formation of a cranial window. Laser speckle contrast imaging (LSCI) has been employed when monitoring blood flow in cerebral arterioles and achieving reperfusion [16].

Methods

Animals and Surgery

Male outbred CD-1 mice (RRID:IMSR_CRL:022, 14–15 weeks old, weight 20–25 g) was used. The mice were obtained from the vivarium of the Rostov Scientific Research Institute of Microbiology and Parasitology (https://rniimp.ru/). Conventional vivarium conditions were used to house 4–5 animals per cage with no restrictions on food or drink and a 12h/12h light/dark cycle. Room temperature was maintained between 22 and 25 °C, and there were 18 air changes per hour. The animals were properly cared for with daily veterinary examination (body position in space, activity), thermometry, and weighing of each individual throughout the entire housing period and before the start of the experiment.

Before the surgery, an animal is weighted. Based on the weight, the amount of anesthetics and Rose Bengal (Sigma-Aldrich Cat#198.250) to be administered is calculated. Mice were anesthetized by injection of 25 mg/kg telazol and 5 mg/kg xylazine intraperitoneally. Adequate depth of anesthesia was achieved in approximately 15 min. The depth of anesthesia was assessed by the absence of plantar reflex and response to pinching of the interfinger membrane, reduction or absence of limb muscle tone, and deceleration of heart and respiratory rates. The following measures of physiological support of the animal during anesthesia and experimental procedures were applied: prevention of dry eyes and corneal damage by moistening with eye drops (during manipulation with the animal the drop kept its position due to surface tension and proportionality of the mouse eye and the drop) and temperature maintenance using the surgical warming system (Rodent Surgical Monitor+, Indus Instruments, USA).

The animal was then mounted in a stereotaxic apparatus. The hair on the head was shaved off, avoiding cutting the vibrissae. The exposed area was treated with an alcohol solution, the skin was dissected (but not cut) and fixed with surgical clips in the desired position, and the periosteum

was removed. Thinning of the cranial bone was not performed, because the target vessel is visible through it with the unaided eye (even in 30 g weight individuals, despite the fact that the bone loses transparency with maturation). To prevent the bone surface from drying out, interfering with irradiation and photographing, sterile normal 0.9% NaCl saline was applied to it when it was necessary.

Before the irradiation, the "wide shot" photograph of vessels was taken under a microscope to select the target vessel (Fig. S1 in Supplementary). The image of initial state was recorded using a microscope camera before irradiation. Vessel selection was guided by the computer model of mouse brain vessels presented in [17]. For the irradiation, we selected arterial vessels lying in the primary sensorimotor cortex regions S1BF (barrel field) and S1FL (forelimb region).

Photothrombosis of Mouse Cortical Arterioles

In order to thrombose the vessel, we used photodynamic effect initiated by photoactivation of Rose Bengal intravascular dye (15 mg/kg or 30 mg/kg of animal weight depending on the vessel size), which was prepared ex tempore. Anesthetized animals were injected slowly into the tail vein. The volume of the administered substance was no more than 0.1 ml per animal weight 20 g [18]. It is acceptable to inject the drug up to 0.2 ml per the same weight of the mouse [19]. If the vessel was not clearly visible, the tail of the animal was immersed for several minutes in warm water (up to 50 °C). To avoid blood loss, the tail at the injection site was loosely tied with a gauze swab. Irradiation was performed within 5 min following the photosensitizer administration since Rose Bengal decreases its activity after 10 min [20]. Photoactivation of Rose Bengal in the target vessel was performed with focused green laser light ($\lambda = 532$ nm, $P = 2.4$ or 3.7 mW, $\varnothing = 1$ mm), for different time intervals (30, 40, 45, 55 s, 3 min, 5 min). After irradiation, the animal was put back under the microscope or LSCI experimental setup (Fig. 1). Changes were captured using the microscope camera immediately after irradiation (video, at least 10 min long), and at other time intervals (45 min, 1.5 h, 3 h), when necessary. Preliminary selection of conditions was performed with the help of Altami CM0745 microscope (Russia) with digital camera for image and video capture of changes in vessels. Control groups included animals subjected to the same procedures but without photosensitizer administration.

Postoperative Period

After the surgery, each animal was placed in a separate warm clean cage until it completely recovered from anesthesia. Further postoperative care included administration of analgesics, antimicrobials, and daily monitoring of the animals' condition for signs of pain and distress; special attention was paid to the condition of sutures and irradiation area. The mice were decapitated at different time intervals after laser irradiation (1, 24 h, 3, 7 days) and the brain was extracted for light, fluorescence, and electron microscopy.

Laser Speckle Contrast Imaging (LSCI)

To record the occurrence of erythrocyte movement and monitor changes in blood flow in the studied brain area, the laser speckle contrast imaging (LSCI) method was used (Fig. 1a). To illuminate the object in the LSCI channel, we used the LDM785 laser source (Thorlabs, USA) with a wavelength of 785 nm. The speckle pattern was recorded with a monochrome CMOS camera UI-3360CP-NIR-GL Rev 2 (IDS GmbH, Germany) (Fig. S2 in Supplementary). To obtain images with more detail, the MY5X-802—5X magnification objective (Mitutoyo, Japan) coupled with an AC254-075-AB-ML achromatic doublet (Thorlabs, USA) was used.

The experimental protocol consisted of several stages: data recording before photothrombotic agent exposure, immediately after the exposure, and 30–50 min after the exposure. In the absence of positive dynamics in the investigated vessel, the measurement was performed 3 h after the occlusion or 24 h later. At least 3 recordings of 5 min in length for each stage of the study were recorded in the LSCI channel; the camera recording rate was 90 frames per second with 11 ms exposure time.

LSCI Data Processing

The initial speckle images were processed with an algorithm developed using MATLAB R2018b (RRID:SCR_001622) software kit. It allows obtaining a dynamic picture of speckle contrast changes. To analyze the data obtained via LSCI, we applied a temporal algorithm for processing 10-s frame sequences (total of 1000 frames per sequence), so the values in each pixel of the image were averaged over 1000 frames [21]. The mean speckle contrast value K is calculated by the formula:

$$K = \frac{\sigma}{< I >} \quad (1)$$

Where $<^{>}$ is the averaging symbol, $<I^{>}$ is the mean intensity value, and σ is the intensity standard deviation.

To visualize the study area, the values of the calculated contrast in the images were converted into pseudo-colors, where red corresponded to high speed of the scattering particle flow (low contrast) and, respectively, blue corresponded to low speed (high contrast). In this study, the LSCI contrast values were converted into LSCI perfusion values using the

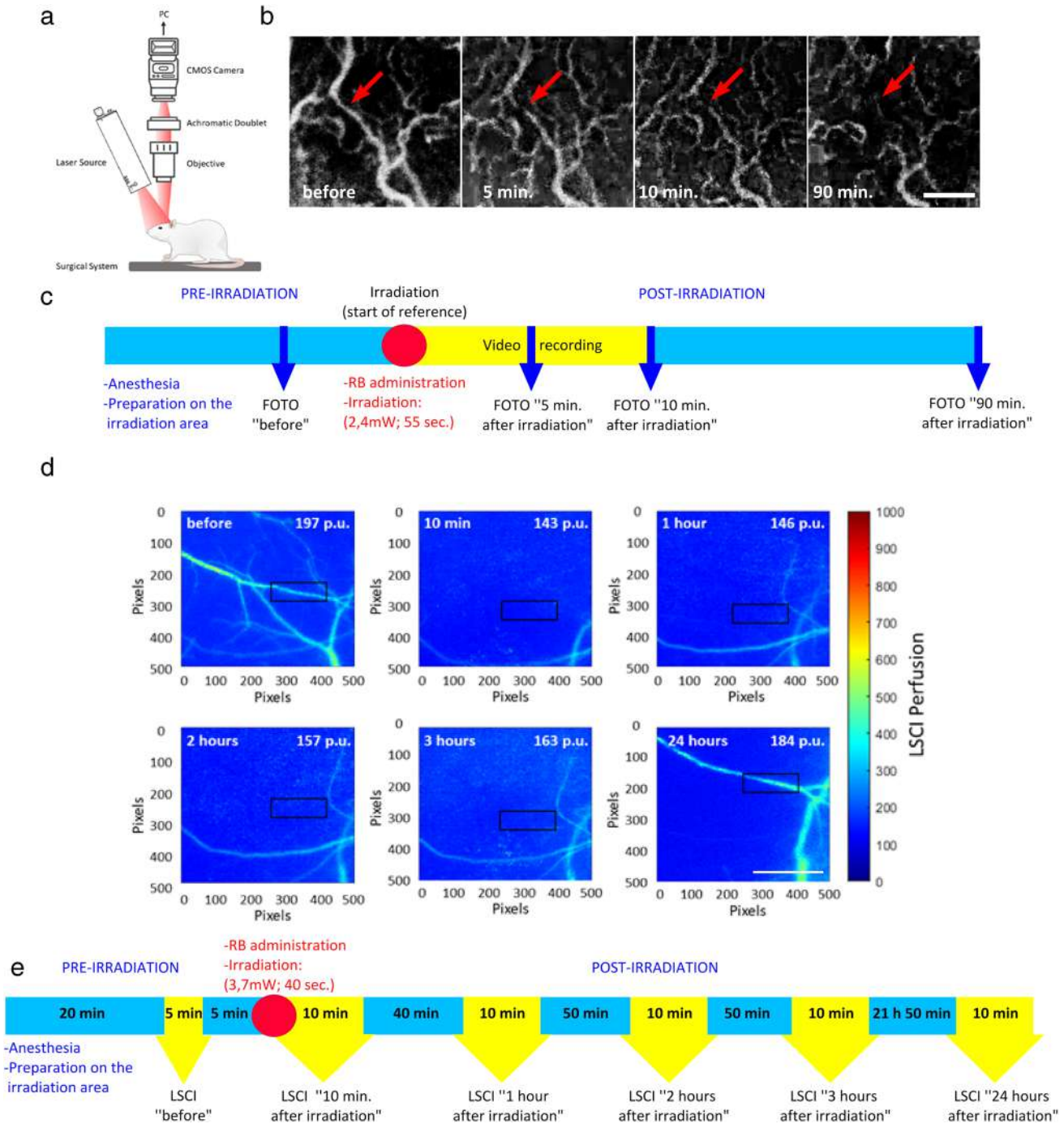

Fig. 1 Photothrombotic ischemia–reperfusion of mouse cerebral cortical arterioles with microinfarct formation. **a** Schematic of the LSCI setup. **b** Target vessel before irradiation, 5, 10, and 90 min after administration of Rose Bengal (RB, 15 mg/kg, i.v.) and irradiation ($\lambda = 532$ nm, $P = 2.4$ mW, $\varnothing = 1$ mm, 55 s). The arrow indicates the site of vessel thrombosis. Scale bar is 100 µm. **c** Timing of experiments of selecting conditions for producing photothrombotic-reperfusion injury of mouse cortical arterioles with microinfarct formation. **d** Laser speckle-contrast imaging of photothrombotic ischemia and reperfusion of mouse cortical arterioles before irradiation and at 10 min, 1, 2, 3, and 24 h after irradiation (RB, 15 mg/kg i.v., $\lambda = 532$ nm, $P = 3.7$ mW, $\varnothing = 1$ mm, 40 s). The rectangle indicates the area of interest (the site of vessel thrombosis). Scale bar is 100 µm. **e** LSCI experiments timing

formula $1/K^2$; quantified results are presented in perfusion units (p.u.) [16, 22].

Light Microscopy

For the paraffin section preparation, animals were decapitated, and the brains were placed in 10% buffered formalin with pH 7.2. Then they were dehydrated in alcohols of increasing concentration (50, 70, 80, 96, and 100%, 10 min each) and xylene and embedded in paraffin. A total of 6–8-μm thick slices were made on an HM 325 Thermo Scientific (RRID:SCR_020259, Germany) rotary microtome and mounted on slides, deparaffinized with xylene and ethanol (100 and 96%) (2 × 3 min), washed with water, and stained with hematoxylin and eosin.

Electron Microscopy

Brain tissue samples of 3 × 3 × 3 mm size were immersed in 2.5% glutaraldehyde (Aurion, USA) for fixation for 24 h. The samples were then washed in phosphate buffer, and additionally post-fixed in 1% OsO_4 solution on phosphate buffer for 1.5 h. The samples were then dehydrated in ascending concentrations of alcohols and absolute ethanol, treated in three changes of propylene oxide, and encapsulated in Epon-812-based epoxy resin. Single and serial ultrathin slices made using Leica EM UC 6 ultramicrotome (RRID:SCR_020226, Germany) with ultra 45° diamond knife (Diatome, Switzerland), were contrasted with uranyl acetate and lead citrate and viewed under a Jem-1011 electron microscope (Jeol, Japan) with 80 kV accelerating voltage.

Immunofluorescence Microscopy

The isolated mouse brain was fixed in 4% paraformaldehyde overnight and placed in 30% sucrose solution. Frontal 20-μm-thick brain slices obtained with a Leica VT1000S vibratome (RRID:SCR_016495, Germany) were washed in PBS and incubated in 5% bovine serum albumin with 0.3% TritonX-100 in PBS for 1 h at room temperature and then incubated overnight at 4 °C in the same BSA solution with antibody added: anti-NeuN (neuronal marker, Merk Cat# MAB377A5, RRID:AB_2814948 or Cat# SAB5700017, RRID:AB_3083690, both 1:1000), anti-GFAP (astrocyte marker, Merk SAB4200571, 1:1000), anti-Iba-1 (microglia marker, Merk Cat# SAB2702364, RRID:AB_2820253, 1:500), anti-CD68 (activated microglia marker, Atlas Antibodies Cat# AMAb90873, RRID:AB_2665705, 1:500). Hoechst 33,342 was used as a cell nuclei marker. After washing in PBS, slices were incubated for 1 h with fluorescent secondary anti-rabbit CF488A (SAB4600045, 1:1000) or anti-mouse CF555 (SAB4600302, 1:1000) antibodies. Negative controls were without no primary antibodies. The slices were then mounted on slides in 60% glycerol/PBS. The results of staining were analyzed using a Nikon Eclipse FN1 fluorescence microscope (RRID:SCR_014995) with a 5MP CCD camera or Olympus BX51 fluorescence microscope (RRID:SCR_023069, Japan) with Hamamatsu ORCA Flash4.0 LT CMOS camera (RRID:SCR_021971, Japan).

Apoptotic Cell Number Estimation

Apoptotic cells were visualized via TUNEL (TdT-mediated dUTP-X nick end labeling) method, labeling DNA strand breaks using "In Situ Cell Death Detection Kit, TMR red" (#12,156,792,910, Roche). The slices were treated with kit reagents according to the manufacturer's recommendations, supplemented with Hoechst 33,342 at a final concentration of 10 μg/ml, and incubated for 1 h at 37 °C. The apoptotic index (AI) was calculated from TUNEL-positive cells (red fluorescence) in the perifocal area and in the cortex of sham-operated animals along the entire perimeter of the micropreparation at × 20 magnification by the formula: AI = [[Number of TUNEL-positive cells] / [Total number of cells (stained with Hoechst 33,342)]] × 100.

Statistical Analysis

Statistical differences between groups with normally distributed data were estimated using one-factor ANOVA with Tukey's test. The Mann–Whitney *U*-test was used to compare groups with distribution other than normal (using the Kruskal–Wallis test to compare three or more groups). Differences were considered significant at $p < 0.05$. Data were presented as mean ± SEM.

Artwork

The figures were designed in PaintShop Pro (RRID:SCR_000338) and Corel Xara 2.

Results

Photothrombosis and Spontaneous Blood Flow Restoration in Arteriole of Mouse Cerebral Cortex with Microinfarct Formation

When selecting the conditions, the light source was the same in all variants (2.4 mW). The selection of conditions was performed using different concentrations of Rose Bengal (15, 30 mg/kg of animal weight), the optimal photosensitizer concentration was 15 mg/kg of animal weight. The irradiation time also varied (45, 50, 55, 60 s), the most successful was the interval of 55 s. Under these conditions, the initial occlusion of the target vessel was observed 5 min after irradiation (Fig. 1a, b). At 10 min after irradiation, the occlusion increase was observed (Fig. 1b). In 90 min, the irradiated part of the target vessel was no longer visible (Fig. 1b).

According to the LSCI data, increasing the laser power to 3.7 mW and decreasing the irradiation time to 40 s while keeping other parameters unchanged (Rose Bengal concentration 15 mg/kg, the same laser) allows obtaining a result comparable to the result under the conditions described above (2.4 mW, irradiation time 55 s). To quantify the visual LSCI results, hereinafter, the area of interest was introduced (a black rectangle in images); LSCI perfusion values were calculated as a mean value inside those chosen areas of interest. In the image before irradiation, the target artery is clearly visible (Fig. 1d), LSCI perfusion is 197 p.u. Ten minutes after irradiation, the target vessel was not observed via LSCI (Fig. 1d) with the overall LSCI perfusion of 143 p.u., indicating no active erythrocyte movement. 1, 2, and 3 h after irradiation, there was no recovery of blood flow (Fig. 1d) with LSCI perfusion that equals 146 p.u., 157 p.u., and 163 p.u., respectively. Reperfusion of the target vessel was observed 24 h after irradiation (Fig. 1d) and as a result, LSCI perfusion increased to 184 p.u.

Prolonged thrombosis of the arteriole resulted in the formation of an expressed microinfarction (Fig. 2a), which was characterized by areas of total death and lysis of nervous tissue and, at the ultrastructural level, in the form of destroyed electron-transparent cell structures and their outgrowths with complete loss of content in the form of organelle remainders into the intercellular space (Fig. 2c). H&E staining showed thinning and weak staining of brain tissue and ischemically altered hyperchromic neurons by as early as 24 h and the presence of cavitations by 3 days (Fig. 2b). In 3 days, the core of the microinfarct zone was invaded by Iba1 and CD68-positive branched macroglia (Fig. 2d), and in 7 days, the formation of a pronounced astrocytic scar was observed (Fig. 2e). Thus, intravenous injection of Rose Bengal at a dose of 15 mg/kg and irradiation of mouse cerebral cortical arterioles with 2.4 mW or 3.7 mW laser beam for 55 or 40 s, respectively, cause similar ischemia–reperfusion lesions resulting in microinfarct formation, because blood flow recovery was observed only 24 h after arteriolar occlusion.

Photothrombosis and Spontaneous Blood Flow Restoration in Mouse Cerebral Cortical Arteriole Without Microinfarct Formation

When selecting the conditions, the light source was the same in all variants (2.4 mW). The selection of conditions was conducted using different concentrations of Rose Bengal (15, 30 mg/kg of animal weight), with 15 mg/kg of animal weight proving to be the optimal concentration. The irradiation time during the selection of conditions was 20, 30, 45, and 50 s, with the optimal interval being 45 s. Under such conditions, occlusion of the target vessel was observed 5 min after irradiation (Fig. 3a, b). Ten minutes after the irradiation, the beginning of blood flow recovery was recorded (Fig. 3a), and 45 min later the blood flow was fully restored (Fig. 3a). According to LSCI data, increasing the laser power to 3.7 mW and decreasing the irradiation time to 30 s with unchanged Rose Bengal concentration (15 mg/kg) allows obtaining a result comparable with the result under the irradiation parameters described above (power 2.4 mW, 45 s). After irradiation, the absence of blood flow in one of the branches of the arteriole was recorded (Fig. 3c). It is also proved by the decrease of LSCI perfusion values (206 p.u. versus 120 p.u.). After 10 min, the blood flow of the whole target vessel was suspended (Fig. 3c) with the LSCI perfusion of 135 p.u., but 60 min after irradiation, blood flow in this area recovered (Fig. 3c), indicating successful short-term TIA. The LSCI perfusion almost returned to its original value as it increased to 190 p.u.

The structure of the cortical tissue of the perifocal area of the injured vessel differed insignificantly from the control one. H&E staining did not reveal significant neuropil changes in the areas adjacent to the vessel (Fig. 4a). However, immunofluorescence staining with antibodies to NeuN (Fig. 4b), as well as H&E staining, revealed the presence of ischemically altered hyperchromic neurons in the perifocal area of the injured arteriole (Fig. 4a). The ultrastructural study of brain samples from the control group of animals showed that the tissue was constituted by an unchanged neuropil with localization of single nerve cells within (Fig. 4c). Neuron nuclei have a regular rounded shape, filled with despiralized chromatin, containing 1–2 nuclei. A neuron itself has a light cytoplasm with distinguishable rough endoplasmic reticulum (RER), ribosomes, mitochondria, and microtubules. Typically, neurons were surrounded by gliofibrils of astrocytes and myelinated axon fibers cut lengthwise and crosswise (Fig. 4c). At the single neuron level, after occlusion and reperfusion of arterioles, we observed vacuolization and destruction of cytoplasm organelles (mitochondria, RER, lamellar complexes), invagination and deformation of the karyolemma, and partial fragmentation of the karyoplasm (Fig. 4c). At the level of individual microcapillaries, detachment of the neuropil from the microcapillary walls is observed, with individual fragments of blood cells in the lumen (Fig. 4c). The walls of microcapillaries themselves are thinned without signs of astroglial perivascular coupling. We could not detect significant cell loss in the perifocal area of the injured vessel 3 days after arteriolar thrombosis (Fig. 4e). Although we observed astrocyte and microglial activation in the proximity of the injured vessel in the first day after TIA (Fig. 4d, e), we did not detect astroglial scar formation (Fig. 4e) or the infiltration by CD68-positive microglia cells at 3 or 7 days after TIA. Increased expression of Iba1 in vascular tissue in response to ischemic arterial injury associated with cytokine release by endothelial cells and vascular smooth muscle cells has

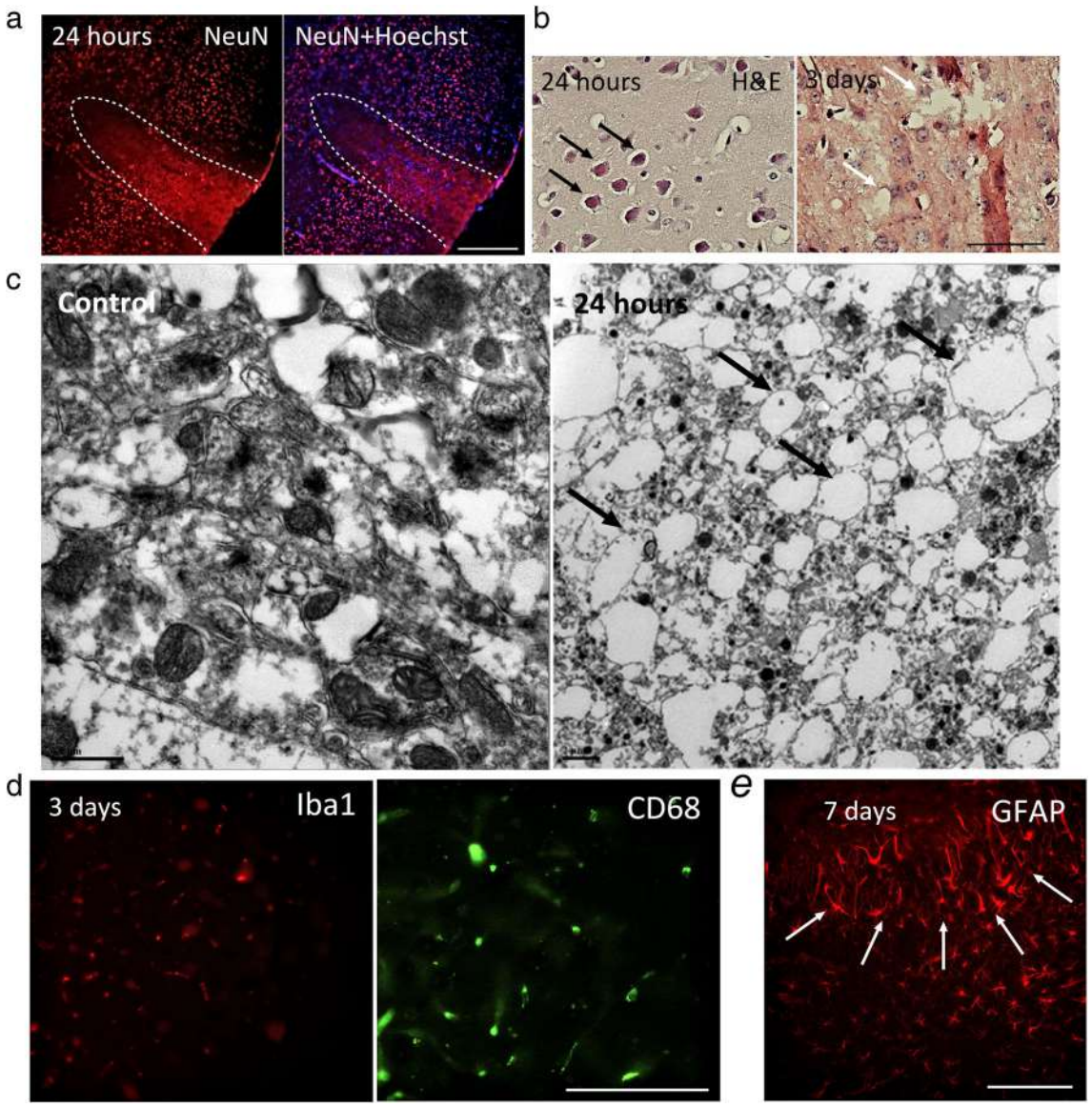

Fig. 2 A view of animal brain cortex after arteriolar occlusion and reperfusion with the microinfarct formation. Exposure conditions: Rose Bengal, 15 mg/kg; λ, 532 nm; P, 2.4 mW; ⌀, 1 mm; irradiation time, 55 s. **a** Animal brain cortex 24 h after irradiation when staining slices with antibodies to NeuN (marker of neurons) and combined fluorescence images when staining for NeuN and Hoechst (marker of nuclei). The dotted line indicates the microinfarct area. Scale bar is 200 μm. **b** Animal cerebral cortex 24 h after arteriolar occlusion and reperfusion when stained with hematoxylin and eosin (black arrows indicate hyperchromic neurons) and 3 days after irradiation (white arrows indicate areas of neuropil cavitation). Scale bar is 100 μm. **c** Ultrastructure of the neuropil of control animal samples (magnification × 80,000) and necrotic changes in brain tissue 24 h after arteriolar irradiation (black arrows indicate areas of cytoplasm vacuolization). Magnification × 10,000. **d** Animal brain cortex 3 days after arteriolar occlusion and reperfusion when stained with antibodies to the microglia markers Iba1 and CD68. Scale bar is 50 μm. **e** View of the cerebral cortex of animals 7 days after arteriolar occlusion and reperfusion when stained with antibodies to GFAP. Arrows show the area of astrocytic scar. Scale bar is 100 μm

been observed, consistent with other studies [23–25]. Thus, intravenous administration of Rose Bengal at a dose of 15 mg/kg and irradiation of mouse cerebral cortical arterioles with 532 nm laser (⌀ 1 mm) at 2.4 mW for 45 s or at 3.7 mW for 30 s, cause similar ischemia–reperfusion injuries that do not result in microinfarction, because blood flow recovery occurs as early as 30 min after arteriolar occlusion.

Discussion

In summary, we demonstrate that intravenous injection of Rose Bengal at a dose of 15 mg/kg and irradiation of mouse cerebral cortical arterioles with a 532 nm wavelength and 1 mm diameter, 2.4 mW or 3.7 mW laser power for 55 or 40 s, respectively, cause similar ischemic-reperfusion damage

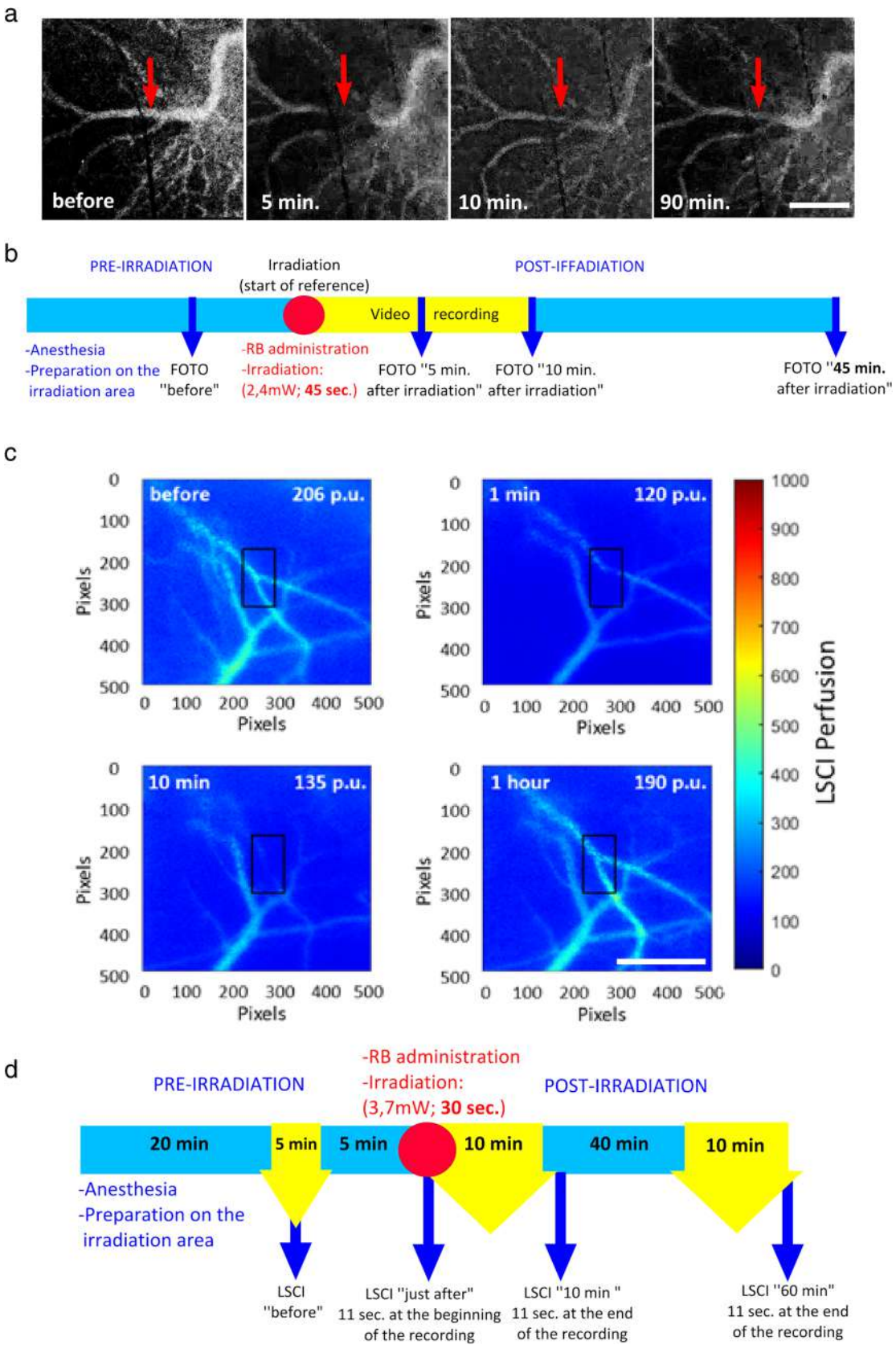
a
before
5 min.
10 min.
90 min.
b
PRE-IRRADIATION
Irradiation
(start of reference)
POST-IFFADIATION
Video
recording
-Anesthesia
-Preparation on the irradiation area
FOTO "before"
-RB administration
-Irradiation:
(2,4mW; 45 sec.)
FOTO "5 min. after irradiation"
FOTO "10 min. after irradiation"
FOTO "45 min. after irradiation"
c
before 206 p.u.
1 min 120 p.u.
10 min 135 p.u.
1 hour 190 p.u.
Pixels
LSCI Perfusion
d
PRE-IRRADIATION
-RB administration
-Irradiation:
(3,7mW; 30 sec.)
POST-IRRADIATION
20 min
5 min
5 min
10 min
40 min
10 min
-Anesthesia
-Preparation on the irradiation area
LSCI "before"
LSCI "just after" 11 sec. at the beginning of the recording
LSCI "10 min " 11 sec. at the end of the recording
LSCI "60 min" 11 sec. at the end of the recording

◂**Fig. 3** Photothrombotic ischemia–reperfusion of mouse cerebral cortical arterioles without microinfarct formation. **a** Target vessel before irradiation, 5, 10, and 90 min after administration of Rose Bengal (RB, 15 mg/kg, i.v.) and irradiation ($\lambda = 532$ nm, $P = 2.4$ mW, $\varnothing = 1$ mm, 45 s). The arrow indicates the site of vessel thrombosis. Scale bar is 100 μm. **b** Timing of experiments of selecting conditions for producing photothrombotic-reperfusion injury of mouse cortical arterioles without microinfarct formation. **c** Laser speckle-contrast imaging of photothrombotic ischemia and reperfusion of mouse cortical arterioles before irradiation and at 1, 10, and 60 min after irradiation (RB—15 mg/kg i.v., $\lambda = 532$ nm, $P = 3.7$ mW, $\varnothing = 1$ mm, 30 s). The rectangle indicates the area of interest (the site of vessel thrombosis). Scale bar is 100 μm. **d** LSCI experiments timing

leading to microinfarct formation. Reducing the exposure time by 10 s (to 45 and 30 s, respectively) while maintaining the same conditions (Rose Bengal dose: 15 mg/kg, laser power 2.4 mW and 3.7 mW, respectively) caused photothrombosis of the arteriole with reperfusion in less than 1 h. This mode of photodynamic exposure caused ischemic changes in neurons at the cellular and subcellular level, and also promoted the activation of astrocytes and microglia cells, in the first day, but not in days following irradiation, which, however, did not lead to the formation of microinfarcts. This mode of photodynamic exposure most accurately reproduced human TIA, which is characterized by the absence of microinfarcts. Thus, by varying the laser power and irradiation time we have achieved the ischemia–reperfusion damage of mouse cerebral cortical arterioles "with" and "without" microinfarct formation with minimal surgical intervention. The use of the LSCI method allowed for the real-time assessment of blood flow in brain microvessels without cranial window formation. In developing the TIA model, we for the first time used the LSCI method for non-invasive recording of the microcirculation. The use of the LSCI method allowed for the real-time assessment of blood flow in brain microvessels without cranial window formation (transcranial), which reduces the risk of complications and allows for multiple measurements. The high spatial resolution of the method makes it possible to obtain detailed images of blood flow in the brain, which is especially useful for localization and analysis of ischemia–reperfusion lesions. At the same time, LSCI provides not only information about the morphology of the vascular bed but can also be used to analyze changes in blood flow velocity when using the developed microinfarct model. It is important that, in comparison with other imaging methods, the equipment for LSCI is more compact and accessible, which facilitates its use in experimental and clinical settings.

RB was used as a photosensitizer. It was shown earlier that compared to fluorescein isothiocyanate (FITC) the formation of reactive oxygen species, especially singlet oxygen species, and blood flow arrest is more intensive when RB is used [26]. Probably, it is the proinflammatory properties of ROS that can explain the activation of astrocytes and microglia in the first day after TIA even in case of minor neuronal loss and without microinfarct formation [27]. The minimal invasiveness of surgery and blood flow detection using LSCI prevents inflammation from being activated in TIA modeling in later periods. However, it should be noted that, in contrast to models using multiphoton excitation, the single-photon RB excitation used in our model leads to ischemia–reperfusion damage of superficial brain vessels. Besides, since the area covered by the laser beam is quite extensive (about 1 mm^2), nearby tissues and vessels are exposed to the irradiation, which may lead to their damage. Therefore, it is necessary to evaluate the laser power before surgery. When irradiating arterioles, there is a possibility of exposure to an adjacent or inferior vessel, resulting in greater damage. This factor should be considered when selecting the target vessel. First, preliminary microscopy of the irradiated area is necessary so that the vessel type can be identified even visually: arteriole or venule. Secondly, it is necessary to choose a vessel far from other vessels. As our experiments have shown, if these conditions are met, the effect of secondary occlusion can be minimized. In 30% of cases, the location of vessels was not suitable for our studies: an arteriole did not lie in the area under study, or the vessels were located very close. In other cases, the vascular network in mice was sparse and it was possible to select such a segment of an arteriole, irradiation of which would not cause occlusion of neighboring vessels. Neither by LSCI method, nor histologically, no damage of neighboring vessels was detected (Figs. 3 and 4). And cell death with increasing intensity and time of irradiation led to the formation of microinfarction in the district of the damaged target vessel (Fig. 2a). In our work, we used outbred CD-I mice, and modeling of TIA was considerably complicated by the fact that the location of arteries and their diameter varied greatly in all individuals. In some individuals, suitable arteries in the target region may not have been observed at all. The use of linear animals may reduce this factor.

Another limitation is that in our work we used young mice, whose skull bones are quite transparent, which may distort the results of our observations when studying the pathogenesis of neurodegeneration and microinfarct formation in old animals [28]. However, the TIA model with microinfarct formation that we developed can be used in mouse lines with early onset of neurodegenerative diseases, such as the early amyloidosis model APP/PS1 mouse line (Tg(APPswe,PSEN1dE9) 85Dbo) and others. The low invasiveness of the surgeries will contribute to better survival of debilitated animals. In addition, the possibility of modeling recurrent TIA, which is difficult with the currently available TIA models [9], is also important.

In humans, TIAs can occur without noticeable damage [29], however, multiple ischemic episodes are not uncommon [30], which can lead to more damage, especially if

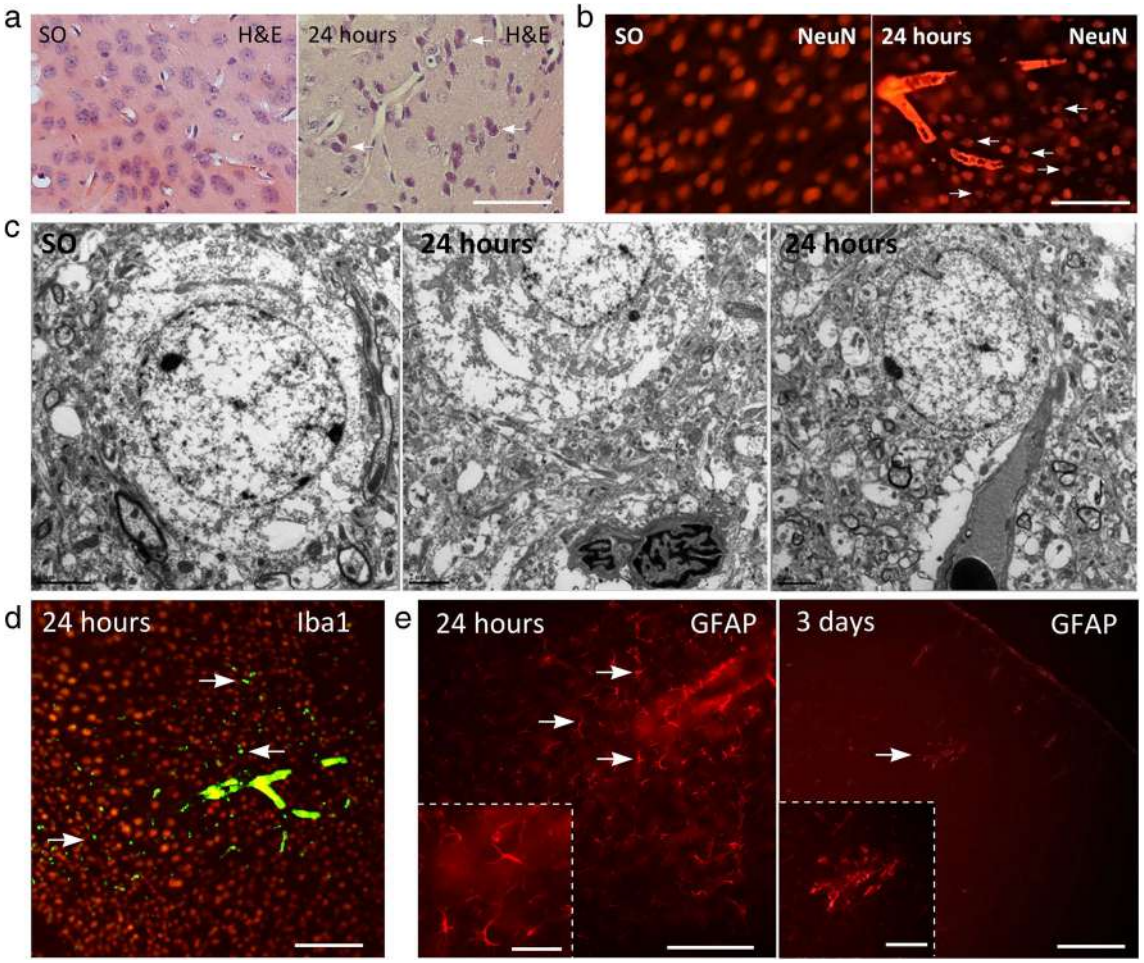

Fig. 4 A view of animal brain cortex after arteriolar occlusion and reperfusion without the microinfarct formation. Exposure conditions: Rose Bengal, 15 mg/kg; λ, 532 nm; *P*, 2.4 mW; ⌀, 1 mm; irradiation time, 45 s. **a** The cerebral cortex of control sham-operated animals (SO) and 24 h after arteriolar occlusion and reperfusion. Hematoxylin and eosin staining. Neuropil cavitation is absent, ischemically altered hyperchromic neurons are visible (white arrows). Scale bar is 100 μm. **b** The cerebral cortex of control animals (SO) and 24 h after irradiation when slices are stained with antibodies to NeuN (marker of neurons). Numerous crumpled neurons are visible (white arrows). Scale bar is 200 μm. **c** Ultrastructure of an intact neuron from a control group of animals (SO). Magnification × 20,000. Ultrastructural changes of neuron and neuropil in the brain tissue of the experimental group of animals 24 h after arteriolar injury. At the level of individual microcapillaries, detachment of neuropil from the microcapillary walls is observed, with individual fragments of blood cells in the lumen (Foto 3). Magnification × 15,000. Exposure conditions: Rose Bengal, 15 mg/kg; laser wavelength, 532 nm; power, 3.7 mW; beam ⌀, 1 mm; irradiation time, 30 s. **d** Animal brain cortex 24 h after arteriolar occlusion and reperfusion when stained with antibodies to the microglia markers Iba1. Scale bar is 100 μm. **e** Animal cortex 24 h and 3 days after arteriolar occlusion and reperfusion when stained with antibodies to GFAP (arrows show areas of activated astroglia). Scale bar, 100 μm; in the embeddings, 50 μm. Exposure conditions: Rose Bengal, 15 mg/kg; laser, 532 nm/2.4 mW/⌀ 1 mm; irradiation time, 45 s

the same arterial distribution is affected [8]. Therefore, we plan to investigate recurrent TIAs in the developed mouse model.

Supplementary Information The online version contains supplementary material available at https://doi.org/10.1007/s12975-024-01285-2.

Acknowledgements The study was supported by the Ministry of Science and Higher Education of the Russian Federation, grant no. FENW-2023-0018 (Kalyuzhnaya Y.N., Logvinov A.K., Demyanenko S.V.), and by Russian Science Foundation, grant no. 22-75-10088 (Golubova N.V., Seryogina E.S., Potapova E.V., Dremin V.V., Dunaev A.V.).

Author Contribution All authors contributed to the study conception and design. Y.N.K and S.V.D. performed surgeries and immunofluorescence microscopy. A.K.L. performed electron microscopy and S.G.P. performed light microscopy. N.V.G., E.S.G., E.V.P., V.V.D., and A.V.D. provided technical support and equipment for the TIA model development and LSCI monitoring in Orel State University. The joint project was supervised by S.V.D. and A.V.D. The first draft of the manuscript was written by Y.N.K. and S.V.D., and all authors commented on previous versions of the manuscript. All authors read and approved the final manuscript.

Funding The study was supported by the Ministry of Science and Higher Education of the Russian Federation, grant no.

FENW-2023–0018 (Kalyuzhnaya Y.N., Logvinov A.K., Demyanenko S.V.), and by Russian Science Foundation, grant no. 22–75-10088 (Golubova N.V., Seryogina E.S., Potapova E.V., Dremin V.V., Dunaev A.V.).

Data Availability No datasets were generated or analysed during the current study.

Declarations

Ethics Approval The study has followed all the applicable standards, including international, national, and institutional guidelines for keeping and using laboratory animals. All experimental procedures were conducted in accordance with the European Union guidelines 86/609/EEC for the use of experimental animals and local legislation for ethics of experiments on animals. The animal protocols were evaluated and approved by the Animal Care and Use Committee of the Southern Federal University (Approval No 3–14/2014; 08/2016 and 02/2022).

Conflict of Interest The authors declare no competing interests.

References

1. Johnston SC. Clinical practice. Transient ischemic attack. N Engl J Med. 2002;347:1687–92.
2. Brazzelli M, Chappell FM, Miranda H, Shuler K, Dennis M, Sandercock PAG, et al. Diffusion-weighted imaging and diagnosis of transient ischemic attack. Ann Neurol. 2014;75:67–76.
3. Albers GW, Caplan LR, Easton JD, Fayad PB, Mohr JP, Saver JL, et al. Transient ischemic attack — proposal for a new definition. N Engl J Med. 2002;347:1713–6.
4. Kleindorfer DO, Towfighi A, Chaturvedi S, Cockroft KM, Gutierrez J, Lombardi-Hill D, et al. 2021 Guideline for the prevention of stroke in patients with stroke and transient ischemic attack: a guideline from the American Heart Association/American Stroke Association. Stroke [Internet]. 2021 [cited 2023 Jun 7];52. Available from: https://doi.org/10.1161/STR.0000000000000375
5. Ham JA, Jeong YJ, Ma MK, Moon HI. The impact of cortical cerebral microinfarcts on functional outcomes in patients with ischemic stroke. Brain Neurorehabil. 2022;15:e30.
6. Wei Y, Pu Y, Pan Y, Nie X, Duan W, Liu D, et al. Cortical microinfarcts associated with worse outcomes in patients with acute ischemic stroke receiving endovascular treatment. Stroke. 2020;51:2742–51.
7. Ejaz S, Emmrich JV, Sawiak SJ, Williamson DJ, Baron J-C. Cortical selective neuronal loss, impaired behavior, and normal magnetic resonance imaging in a new rat model of true transient ischemic attacks. Stroke. 2015;46:1084–92.
8. Qiao M, Zhao Z, Barber PA, Foniok T, Sun S, Tuor UI. Development of a model of recurrent stroke consisting of a mild transient stroke followed by a second moderate stroke in rats. J Neurosci Methods. 2009;184:244–50.
9. Kalyuzhnaya YN, Khaitin AM, Demyanenko SV. Modeling transient ischemic attack via photothrombosis. Biophys Rev. 2023;15:1279–86.
10. Uzdensky AB. Photothrombotic stroke as a model of ischemic stroke. Transl Stroke Res. 2018;9:437–51.
11. Mauritzon S, Ginstman F, Hillman J, Wårdell K. Analysis of laser Doppler flowmetry long-term recordings for investigation of cerebral microcirculation during neurointensive care. Front Neurosci. 2022;16:1030805.
12. Shih AY, Blinder P, Tsai PS, Friedman B, Stanley G, Lyden PD, et al. The smallest stroke: occlusion of one penetrating vessel leads to infarction and a cognitive deficit. Nat Neurosci. 2013;16:55–63.
13. Tuor UI, Deng Q, Rushforth D, Foniok T, Qiao M. Model of minor stroke with mild peri-infarct ischemic injury. J Neurosci Methods. 2016;268:56–65.
14. Yoo H-J, Ham J, Duc NT, Lee B. Quantification of stroke lesion volume using epidural EEG in a cerebral ischaemic rat model. Sci Rep. 2021;11:2308.
15. Chen P, Goldberg DE, Kolb B, Lanser M, Benowitz LI. Inosine induces axonal rewiring and improves behavioral outcome after stroke. Proc Natl Acad Sci. 2002;99:9031–6.
16. Golubova N, Potapova E, Seryogina E, Dremin V. Time–frequency analysis of laser speckle contrast for transcranial assessment of cerebral blood flow. Biomed Signal Process Control. 2023;85:104969.
17. Xiong B, Li A, Lou Y, Chen S, Long B, Peng J, et al. Precise cerebral vascular atlas in stereotaxic coordinates of whole mouse brain. Front Neuroanat. 2017;11:128.
18. Rybakova AV, Makarova MN, Kukharenko AE, Vichare AS, Rueffer FR. Current requirements for and approaches to dosing in animal studies. Bull Sci Cent Expert Eval Med Prod. 2018;8:207–17.
19. Serwer L, Hashizume R, Ozawa T, James CD. Systemic and local drug delivery for treating diseases of the central nervous system in rodent models. J Vis Exp. 2010;1992.
20. Taylor Z, Shih A. Targeted occlusion of individual pial vessels of mouse cortex. BIO-Protoc [Internet]. 2013 [cited 2023 Jun 9];3. Available from: https://bio-protocol.org/e897
21. Potapova EV, Seryogina ES, Dremin VV, Stavtsev DD, Kozlov IO, Zherebtsov EA, et al. Laser speckle contrast imaging of blood microcirculation in pancreatic tissues during laparoscopic interventions. Quantum Electron. 2020;50:33.
22. Mizeva I, Dremin V, Potapova E, Zherebtsov E, Kozlov I, Dunaev A. Wavelet analysis of the temporal dynamics of the laser speckle contrast in human skin. IEEE Trans Biomed Eng. 2020;67:1882–9.
23. Autieri MV, Carbone C, Mu A. Expression of allograft inflammatory factor-1 is a marker of activated human vascular smooth muscle cells and arterial injury. Arterioscler Thromb Vasc Biol. 2000;20:1737–44.
24. Schulze JO, Quedenau C, Roske Y, Adam T, Schüler H, Behlke J, et al. Structural and functional characterization of human Iba proteins. FEBS J. 2008;275:4627–40.
25. Pawluk H, Woźniak A, Grześk G, Kołodziejska R, Kozakiewicz M, Kopkowska E, et al. The role of selected pro-inflammatory cytokines in pathogenesis of ischemic stroke. Clin Interv Aging. 2020;15:469–84.
26. Delafontaine-Martel P, Zhang C, Lu X, Damseh R, Lesage F, Marchand PJ. 2023 Targeted capillary photothrombosis via multiphoton excitation of Rose Bengal. J Cereb Blood Flow Metab. 0271678X2311515.
27. Alsbrook DL, Di Napoli M, Bhatia K, Biller J, Andalib S, Hinduja A, et al. Neuroinflammation in acute ischemic and hemorrhagic stroke. Curr Neurol Neurosci Rep. 2023;23:407–31.
28. Lin X, Fan Y, Zhang F, Lin Y. Cerebral microinfarct is emergency consequence of Alzheimer's disease: a new insight into development of neurodegenerative diseases. Int J Biol Sci. 2022;18:1569–79.
29. Amin HP, Madsen TE, Bravata DM, Wira CR, Johnston SC, Ashcraft S, et al. Diagnosis, workup, risk reduction of transient ischemic attack in the emergency department setting: a scientific statement from the American Heart Association. Stroke. 2023;54:e109–21.

30. Tuor UI, Zhao Z, Barber PA, Qiao M. Recurrent mild cerebral ischemia: enhanced brain injury following acute compared to subacute recurrence in the rat. BMC Neurosci. 2016;17:28.